

# Characteristics of InP HEMT Harmonic Optoelectronic Mixers and Their Application to 60GHz Radio-on-Fiber Systems

Chang-Soon Choi<sup>1</sup>, Hyo-Soon Kang<sup>1</sup>, Dae-Hyun Kim<sup>2</sup>, Kwang-Seok Seo<sup>2</sup> and Woo-Young Choi<sup>1</sup>

<sup>1</sup>Department of Electrical and Electronic Engineering, Yonsei University, Seoul, 120-749, Korea

<sup>2</sup>School of Electrical Engineering, Seoul National University, Seoul, 151-741, Korea

**Abstract** — We present device characteristics of InP HEMT as a harmonic optoelectronic mixer. A single InP HEMT device performs photodetection of optically transmitted data, and frequency up-conversion of them into 60GHz band. Several mixer performance characteristics are investigated and 622Mbps data transmission in 60GHz radio-on-fiber system is successfully demonstrated using InP HEMT harmonic optoelectronic mixer.

**Index Terms** — millimeter-wave, radio-on-fiber system, InP HEMT, optoelectronic mixer, optoelectronic integration.

## I. INTRODUCTION

The needs for broadband wireless communication have grown much interest in millimeter-wave frequency bands, especially 60GHz, because of its wide transmission bandwidth and the possibility of efficient frequency reuse. However, their use is not yet widespread due to difficulties in millimeter-wave generation, transmission and processing. With development of fiber-optic technologies, radio-on-fiber systems which utilize optical fibers as low loss and highly flexible transmission medium have been investigated as a solution for these problems [1].

In millimeter-wave radio-on-fiber systems, a large number of antenna base stations are located within the coverage of a single central office in order to compensate high transmission loss of millimeter-waves. Consequently, it is important to come up with low cost and simple antenna base station architecture for practical implementation of these radio-on-fiber systems.

One attractive approach is the one-chip integration of a photodetector and other RF components that are required in antenna base station. Indium-phosphide high-electron mobility transistors (InP HEMTs) are very useful devices for this optoelectronic integration because they can perform photodetection to 1.55 $\mu$ m light with high internal gain while maintaining compatibility to conventional MMIC process [2]. In addition, they can provide additional functionalities such as optoelectronic mixing and optical injection-locked oscillation [2-3].

In this paper, we present detailed characteristics of a harmonic optoelectronic mixer based on a single InP HEMT and its application to 60GHz radio-on-fiber systems. The photodetection mechanism for the InP HEMT is first identified and it is experimentally demonstrated that the InP HEMT can be operated as a 60GHz harmonic optoelectronic mixer. Such optoelectronic mixer performance characteristics as internal conversion gain and local oscillator (LO) frequency ranges are investigated and 622Mbps data transmission in 60GHz radio-on-fiber system is demonstrated.

## II. PHOTODETECTION CHARACTERISTICS

Epitaxial layers for the HEMT used for our investigation are schematically shown in Fig. 1. It has a pseudomorphic In<sub>0.65</sub>Ga<sub>0.35</sub>As channel in order to improve electrical device performance at the millimeter-wave operation. With 0.1 $\mu$ m gate-length, it exhibits the maximum transconductance of 720mS/mm, the current-gain cutoff frequency ( $f_T$ ) of 165GHz and the maximum oscillation frequency ( $f_{max}$ ) of 95GHz at the gate bias of -0.4V and the drain bias of 1V.

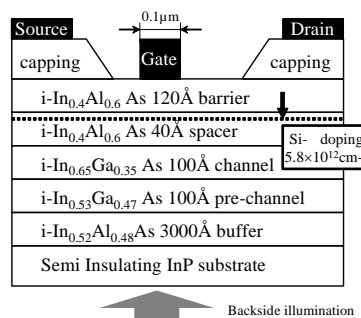


Fig. 1. Layer structure of InP pseudomorphic HEMT

1.55 $\mu$ m photodetection characteristics were analyzed with the semiconductor parameter analyzer (HP4145B), the network analyzer (HP8722D) with optical signals at 1552nm provided by a DFB laser. The light was illuminated from the backside of InP substrate with a

single-mode lensed fiber which provides the coupling efficiency of approximately 10%. Since InP substrate and InAlAs buffer layer are transparent to 1.55 $\mu$ m light, optical absorption occurs only at In<sub>0.65</sub>Ga<sub>0.35</sub>As and In<sub>0.53</sub>Ga<sub>0.47</sub>As channels.

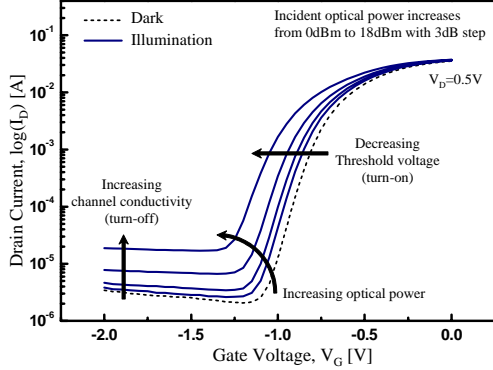


Fig. 2.  $I_D$  versus  $V_G$  under dark and illuminated conditions

Fig. 2 shows measured drain-currents ( $I_D$ ) as a function of gate-voltages ( $V_G$ ) under dark and illuminated conditions. The InP HEMT shows a negative shift in threshold voltages as well as increase in  $I_D$  with increasing incident optical powers. It has been reported that these threshold voltage shifts are due to the photovoltaic effect caused by photo-generated holes in the channel [3-5].

Since the gate voltage is effectively modulated with the photovoltaic effect, internal gain is provided making the HEMT a phototransistor. Even when  $V_G$  is lower than the threshold voltage, namely at turn-off condition, small increase in  $I_D$  is observed with illumination as can be seen in the figure. This is due to the photoconductive effect in which photo-generated electrons increase the channel conductivity and, thus, increase  $I_D$ . It should be noted that it does not provide any internal gain since the HEMT is off. These photodetection characteristics are affirmed by Fig. 3 which shows the InP HEMT optical modulation responses for both turn-on and turn-off conditions. Because the photovoltaic effect is dominated by the lifetime of photo-generated holes, the photoresponse for turn-on condition has relatively small optical 3dB bandwidth of about 560MHz. On the other hand, for turn-off condition, the photoresponse has much larger 3dB bandwidth because photoconductive effect is dominated by photo-generated electrons having much short life-time. Since the HEMT does not operate as a transistor in turn-off condition, it performs only photodetection without any internal gain. By utilizing this dependence of photodetection characteristics on bias conditions, we can determine the internal gain provided by the HEMT as a phototransistor by measuring photoresponses at both turn-

off and turn-on conditions under the identical optical illumination condition, and taking their differences as shown in Fig. 3. In our experiments, 38dB internal gain is obtained at 100MHz optical modulation frequency. For its uses as a phototransistor and an optoelectronic mixer, InP HEMT should be at turn-on condition for providing internal gain. These optical modulation responses directly affect the photodetection bandwidth of optically transmitted intermediate frequency (IF) with data. It can be seen from the figure that IF up to the GHz range can have high internal gain, which should be sufficient for many applications.

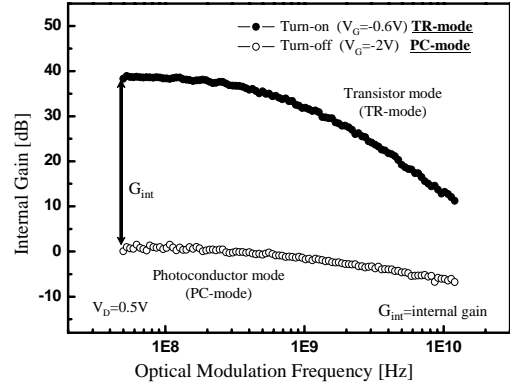


Fig. 3. Optical modulation responses of InP HEMT under turn-on condition ( $V_G = -0.6V$ ) and turn-off condition ( $V_G = -2V$ )

### III. HARMONIC OPTOELECTRONIC MIXING

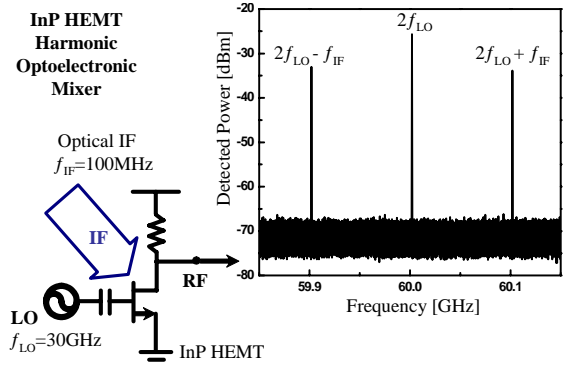


Fig. 4. InP HEMT harmonic optoelectronic mixer and its 60GHz frequency up-conversion spectrum under applying 30GHz LO and optical 100MHz IF.

With a single InP HEMT device, it is possible to realize photodetection and harmonic optoelectronic up-conversion simultaneously [5]. Fig. 4 shows the schematic diagram for utilizing the InP HEMT as a harmonic

optoelectronic mixer and its up-converted output spectrum at 60GHz. It can be seen that there are harmonic optoelectronic mixing products at  $2f_{LO}+f_{IF}$  (60.1GHz) and  $2f_{LO}-f_{IF}$  (59.9GHz) and 2<sup>nd</sup> harmonic of LO at  $2f_{LO}$  (60GHz) with 30GHz LO and optical 100MHz IF. With this harmonic up-conversion, lower frequency LO can be used making the implementation of base station easier.

Conversion gain is an important parameter for the performance of a frequency up-converter. In the case of an optoelectronic mixer, it is difficult to determine the conversion gain accurately since the actually absorbed optical IF power in HEMT is not accurately known. Instead, we define the internal conversion gain which is the power ratio of  $2f_{LO}+f_{IF}$  and  $2f_{LO}-f_{IF}$  optoelectronic up-converted signals to the photodetected  $f_{IF}$  signal without internal gain, which can be measured at turn-off condition as mentioned earlier.

Since the measurement sensitivity at 60GHz band is limited by high background noise level of the external V-band harmonic mixer (Agilent 11974V) used for our measurement, the experiments were first carried out in the 20GHz band with 10GHz LO having 0dBm power and 100MHz optical IF signals. Fig. 5 shows the internal conversion gain for  $f_{LO}+f_{IF}$  and  $2f_{LO}+f_{IF}$  components as a function of  $V_G$ . The photodetected  $f_{IF}$  signal power without internal gain is -49dBm measured at  $V_G=-2V$ . The non-monotonic curves for optoelectronic up-conversion efficiencies are attributed to the nonlinearity of transconductance of the HEMT. It should be noted that the maximum 20dB internal conversion gain for harmonic optoelectronic up-conversion at  $2f_{LO}+f_{IF}$  was obtained at  $V_G$  of -0.9V while suppressing undesired mixing component at  $f_{LO}+f_{IF}$ . In this  $V_G$  condition, the output RF spectra at 10GHz and 20GHz bands are shown in Fig. 6. It can be seen that the output power of  $2f_{LO}+f_{IF}$  is much larger than that of  $f_{LO}+f_{IF}$ .

For its use at millimeter-wave band, we measured the internal conversion gain for  $2f_{LO}+f_{IF}$  as a function of applied LO frequencies and the results are shown in Fig. 7. Measurement was not taken from 40GHz to 50GHz due to the lack of external harmonic mixer for these frequency bands. In our experiments, the InP HEMT as a harmonic optoelectronic mixer exhibits wide LO frequency ranges which are well extended to the millimeter-wave band. The origins for slightly decreased internal conversion gain as increasing LO frequency are due to the reduction in  $S_{21}$  indicating forward power gain and increased loss of RF components which were guaranteed below 50GHz. Nevertheless, the internal conversion gain of 18dB is obtained at 60GHz band.

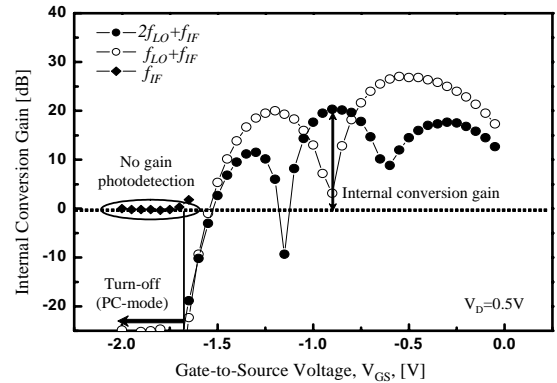


Fig. 5. Internal conversion gain for  $f_{LO}+f_{IF}$  and  $2f_{LO}+f_{IF}$  as a function of gate voltage

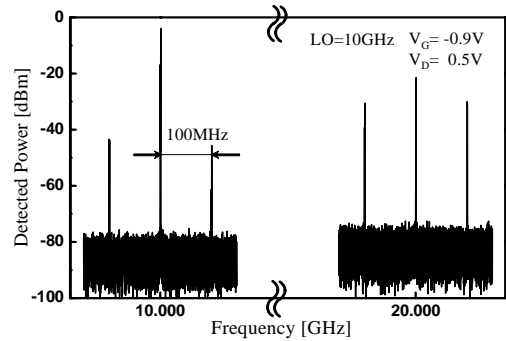


Fig. 6. Output RF spectrum of harmonic optoelectronic up-conversion by InP HEMT with optimum bias conditions,  $V_G=-0.9V$  and  $V_D=0.5V$

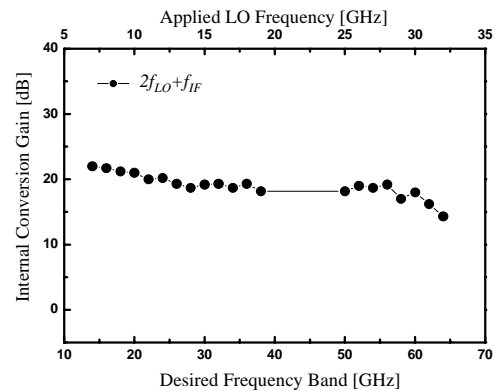


Fig. 7. Internal conversion gain for harmonic optoelectronic up-conversion at  $2f_{LO}+f_{IF}$  as a function of applied LO frequencies.

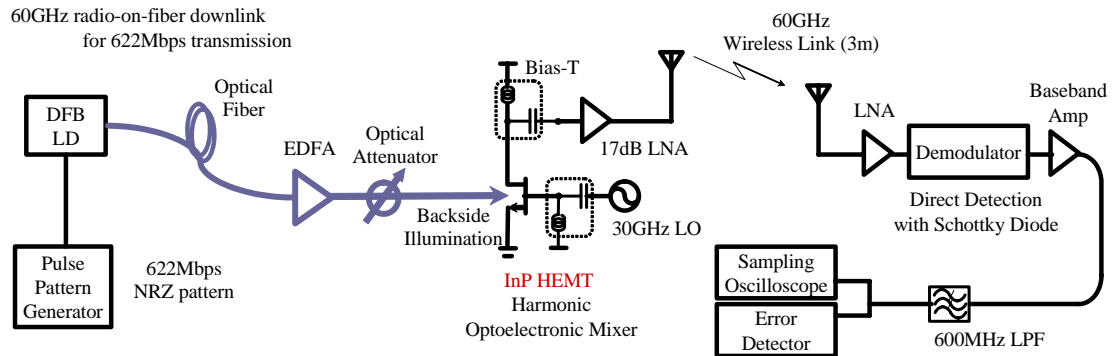


Fig. 8. 60GHz radio-on-fiber systems utilizing InP HEMT as a harmonic optoelectronic mixer

#### IV. 60GHz RADIO-ON-FIBER SYSTEM

To investigate the feasibility of using InP HEMT as a 60GHz harmonic optoelectronic mixer in a radio-on-fiber (RoF) system, a remote up-conversion 60GHz RoF downlink transmission system was constructed as shown in Fig. 8. Optical data channel produced by a DFB laser directly modulated with 622Mbps NRZ pseudo-random bit sequence ( $2^{15}-1$ ) was transmitted from the central station to the base station. The optically transmitted data were then frequency up-converted to 60GHz band using the InP HEMT harmonic optoelectronic mixer with the optimal bias conditions and 30GHz, -6dBm LO. The optimal bias condition was experimentally confirmed to be same as those determined at 20GHz. The output signal at drain port was amplified by 17dB LNA and radiated from the horn antenna with the 20dB gain. After 3m wireless transmission, the received signals were demodulated using the direct detection technique with a Schottky diode. Clear eye-opening was observed for the recovered data as shown in Fig. 9-(A). In addition, the link performance was evaluated by measuring the bit error rate (BER) as a function of coupled-in powers to the InP HEMT, which are estimated to be 10% of incident optical power. Fig. 9-(B) shows the experimental results for BER performance of 60GHz radio-on-fiber links. Error-free transmission was achieved at the coupled-in optical power of 4dBm.

#### V. CONCLUSION

In this work, we investigated characteristics of a InP HEMT as a millimeter-wave harmonic optoelectronic mixer and demonstrated 622Mbps data transmission in 60GHz radio-on-fiber system by utilizing it. Based on the photodetection mechanism in the InP HEMT, we defined internal conversion gain and investigated its dependence

on  $V_G$  for the maximum harmonic optoelectronic mixing efficiency. At 60GHz band, internal conversion gain of 18dB was obtained. It is expected that InP HEMTs can be useful in simplifying antenna base station architecture in 60GHz radio-on-fiber system.

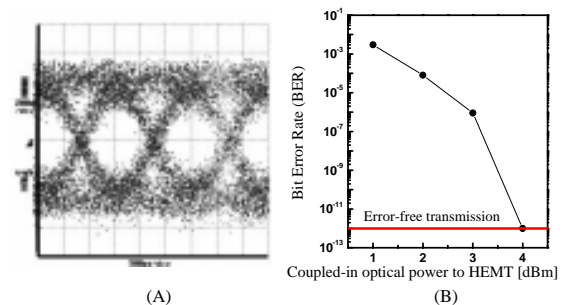


Fig. 9. (A) Eye-diagram for recovered 622Mbps data (B) Bit-error rate as a function coupled-in optical power to HEMT

#### REFERENCES

- [1] A. J. Seeds, "Microwave photonics" *IEEE Trans. Microwave Theory and Tech.*, vol. 50, no. 3, pp. 877-887, Mar. 2002.
- [2] C. Rauscher and K. J. Williams, "Heterodyne reception of millimeter-wave modulated optical signals with an InP-based Transistor," *IEEE Trans. Microwave Theory and Tech.*, vol. 42, no. 11, pp. 2027-2034, Nov. 1994.
- [3] A. Paoella, S. Malone, T. Berceli and P. R. Herczfeld, "MMIC compatible lightwave-microwave mixing techniques," *IEEE Trans. Microwave Theory and Tech.*, vol. 43, no. 3, pp. 518-522, Mar. 1995.
- [4] Y. Takanashi, K. Takahata and Y. Muramoto, "Characteristics of InAlAs/InGaAs high-electron-mobility transistors under illumination with modulated light," *IEEE Trans. Elec. Dev.*, vol. 46, no. 3, pp. 2271-2277, Dec. 1999
- [5] Chang-Soon Choi, Woo-Young. Choi, Dae-Hyun Kim and Kwang-Seok Seo, "A millimeter-wave harmonic optoelectronic mixer based on InAlAs/InGaAs metamorphic HEMT," in *IEEE MTT-S Int. Microwave Symp. Dig.*, pp. 1383-1386, Philadelphia, 2003.

# 2004 Microwave Symposium Technical Program Schedule

## Session TU1A Advances in Low Noise Silicon Technology & Applications

**8:00am – 9:40am**

**Room 200**

**Tuesday, June 8, 2004**

Chair: F. Danneville, University of Lille

Co-chair: A. Riddle, Macallan Consulting

<b>TU1A-1</b>	<b>RF Noise Scaling Trend of MOSFETs from 0.5 um to 0.13 um Technology Nodes</b>	<b>9</b>
<b>8:00 AM</b>	M-C. King, M-T. Yang, C-W. Kuo, Y. Chang, and A. Chin	
<b>TU1A-2</b>	<b>A Low Power DC-7.8 GHz BiCMOS LNA for UWB and Opical Communication</b>	<b>13</b>
<b>8:20 AM</b>	F. Ellinger, D. Barras, M. Schmatz, and H. Jackel	
<b>TU1A-3</b>	<b>Noise Performance of 90 nm CMOS Technology</b>	<b>17</b>
<b>8:40 AM</b>	D. Becher, G. Banerjee, R. Basco, C. Hung, K. Kuhn, and W-K. Shih	
<b>TU1A-4</b>	<b>Low Noise, and High Gain Wideband Amplifier Using SiGe HBT Technology</b>	<b>21</b>
<b>9:00 AM</b>	R. Chan and M. Feng	
<b>TU1A-5</b>	<b>A 12-GHz Heterodyne Receiver for Digital Video Broadcasting via Satellite Applications in Silicon Bipolar Technology</b>	<b>25</b>
<b>9:20 AM</b>	S. Smerzi, T. Copani, G. Girlando, A. Castorina, and G. Palmisano	

## Session TU2A Non Linear Device Modeling

**Room 201BC**

Chair: R. Mallavarpu, Raytheon RF Components

Co-chair: G. Manes, University of Firenze

<b>TU2A-1</b>	<b>Enhanced Prediction of pHEMT Nonlinear Distortion Using a Novel Charge Conservative Model</b>	<b>31</b>
<b>8:00 AM</b>	M. Wren and T.J. Brazil	
<b>TU2A-2</b>	<b>A Symmetric and Thermally-de-Embedded Nonlinear FET Model for Wireless and Microwave Applications</b>	<b>35</b>
<b>8:20 AM</b>	J. Wood and D. Root	
<b>TU2A-3</b>	<b>A New Physics Based Dynamic Electro Thermal Large Signal Model for RF LDMOS FETS</b>	<b>39</b>
<b>8:40 AM</b>	M. Versleijen, V. Bloem, A. van Steenwijk, and O. Yanson	
<b>TU2A-4</b>	<b>Large-Signal HBT Model Requirements to Predict Nonlinear Behaviour</b>	<b>43</b>
<b>9:00 AM</b>	M. Rudolph and R. Doerner	
<b>TU2A-5</b>	<b>Effects of Bias and Load Conditions on Dynamic Self Heating of Bipolar Transistors</b>	<b>47</b>
<b>9:10 AM</b>	S. Cherepko, J. Hwang, and W. Curtice	
<b>TU2A-6</b>	<b>New Nonlinear Device Model for Microwave Power GaN HEMTs</b>	<b>51</b>
<b>9:20 AM</b>	P. Cabral, J. Pedro, and N. Carvalho	

## Session TU3A

# Theory and Design of Power Dividers

### Room BallC

Chair: C. Nguyen, National Science Foundation

Co-chair: A. Fathy, University of Tennessee

<b>TU3A-1</b>	<b>Reconfigurable Power Divider and Combiner with Variable Power Ratio</b>	<b>57</b>
<b>8:00 AM</b>	K.T. Kim, Y. Chung, J.H. Kang, T. Itoh, and D. Ahn	
<b>TU3A-2</b>	<b>3-way Low Loss Phase Combiner for Power Amplifier Sharing in 3-Sector Cellular Networks</b>	<b>61</b>
<b>8:20 AM</b>	C. Metz and T. Baras	
<b>TU3A-3</b>	<b>General Design Equations of N-Way Arbitrary Power Dividers</b>	<b>65</b>
<b>8:40 AM</b>	H-R. Ahn, K. Lee, and N-H. Myung	
<b>TU3A-4</b>	<b>A Design of Multi-Stage, Multi-Way Microstrip Power Dividers with Broadband Properties</b>	<b>69</b>
<b>9:00 AM</b>	M. Kishihara, K. Yamane, I. Ohta, and T. Kawai	
<b>TU3A-5</b>	<b>A Simplified Approach for the Design of Radial Power Combining Structures</b>	<b>73</b>
<b>9:20 AM</b>	A.E. Fathy and D. Kalokitis	

## Session TU4A

# Spatial Power Combining and Quasi-Optical Techniques

### Room 202CD

Chair: K. Mizuno, Tohoku University

Co-chair: J. Hacker, Rockwell Scientific

<b>TU4A-1</b>	<b>A Single Chip Two-stage W-band Grid Amplifier</b>	<b>79</b>
<b>8:00 AM</b>	C-T. Cheung, M. DeLisio, J. Rosenberg, R. Tsai, R. Kagiwada, and D. Rutledge	
<b>TU4A-2</b>	<b>A Ka-Band Grid Amplifier Module with Over 10 Watts Output Power</b>	<b>83</b>
<b>8:20 AM</b>	M. DeLisio, B. Deckman, C-T. Cheung, S. Martin, D. Nakhla, E. Hartmann, C. Rollison, J.B. Pacetti, and J. Rosenberg	
<b>TU4A-3</b>	<b>A Dual Polarized Millimeter-Wave Multibeam Phased Array</b>	<b>87</b>
<b>8:40 AM</b>	A. Al-Zayed, L. Schulwitz, and A. Mortazawi	
<b>TU4A-4</b>	<b>Power Combining by Means of Harmonic Injection Locking</b>	<b>91</b>
<b>9:00 AM</b>	M.R. Kuhn and E.M. Biebl	
<b>TU4A-5</b>	<b>An X-Band Spatial Power Combiner Using a Planar Array of Stacked Patches for Bandwidth Enhancement</b>	<b>95</b>
<b>9:20 AM</b>	F-C.E. Tsai and M.E. Bialkowski	

## Session TU5A

### Mixed signal circuits from 10 to 144Gb/s

#### Room 201A

Chair: S. Marsh, Bookham Technology

Co-chair: J.P. Mattia, Tarkus Consulting

<b>TU5A-1</b>	<b>A 24-Gbps 3-bit Nyquist ADC using InP HBTs for Electronic Dispersion Compensation</b>	<b>101</b>
<b>8:00 AM</b>	H. Nosaka, M. Nakamura, M. Ida, K. Kurishima, T. Shibata, M. Tokumitsu, and M. Muraguchi	
<b>TU5A-2</b>	<b>A 0.18<math>\mu</math>m CMOS Equalizer with Improved Multiplier for 4-PAM/20Gbps Throughput Over 20-inch FR-4 Backplane Channel</b>	<b>105</b>
<b>8:20 AM</b>	M. Maeng, F. Bien, Y. Hur, S. Chandramouli, H. Kim, Y. Kumar, C. Chun, E. Gebara, and J. Laskar	
<b>TU5A-3</b>	<b>10-Gb/s Electrical Backplane Transmission using Duobinary Signaling</b>	<b>109</b>
<b>8:40 AM</b>	J. Sinsky, A. Adamiecki, and M. Duelk	
<b>TU5A-4</b>	<b>DFF-Drivers ICs for 40 Gb/s ETDM in InP DHBT Technology</b>	<b>113</b>
<b>9:00 AM</b>	A. Konczykowska, F. Jorge, M. Riet, S. Blayac, J. Moulu, and J. Godin	
<b>TU5A-5</b>	<b>144-Gbit/s Selector and 100-Gbit/s 4:1 Multiplexer Using InP HEMTs</b>	<b>117</b>
<b>9:20 AM</b>	T. Suzuki, Y. Nakasha, T. Takahashi, K. Makiyama, T. Hirose, and M. Takikawa	

## Session TU6A

### Microwave Superconducting Components and Circuits.

#### Room 202AB

Chair: M. Lancaster, The University of Birmingham

Co-chair: C. Jackson, Raytheon Pace and Airborne Systems

<b>TU6A-1</b>	<b>Hilbert Fractal Curves for HTS Miniaturized Filters</b>	<b>123</b>
<b>8:00 AM</b>	M. Barra, C. Collado, J. Mateu, and J. O'Callaghan	
<b>TU6A-2</b>	<b>An HTS Lumped-Element Notch Filter</b>	<b>127</b>
<b>8:20 AM</b>	K. Dustakar and S. Berkowitz	
<b>TU6A-3</b>	<b>Switched Superconductive Filter-Banks</b>	<b>131</b>
<b>8:40 AM</b>	S.F. Peik, B. Jolley, and R. Mansour	
<b>TU6A-4</b>	<b>Characterizing a Double-Spiralled Meander Superconducting Microstrip Delay Line using a Resonator Technique</b>	<b>135</b>
<b>8:50 AM</b>	H.T. Su, Y. Wang, F. Huang, and M. Lancaster	
<b>TU6A-5</b>	<b>A Superconducting Microwave Power Limiter for High-Performance Receiver Protection</b>	<b>139</b>
<b>9:10 AM</b>	J.C. Booth, K. Leong, and S. Schima	
<b>TU6A-6</b>	<b>HTS Sensors for NQR Spectroscopy</b>	<b>143</b>
<b>9:20 AM</b>	C. Wilker, J.D. McCambridge, D.B. Laubacher, R.L. Alvarez, J.S. Guo, C.F. Carter III, M.A. Pusateri, and J.L. Schiano	

## Session TU1C

### Advances in Low Noise HEMT Technology

1:20pm – 3:00pm

Room 200

Chair: T. Cisco, Raytheon

Co-chair: M. Gupta, San Diego State University

<b>TU1C-1</b>	<b>X-band GaAs mHEMT LNAs With 0.5 dB Noise Figure</b>	<b>149</b>
<b>1:20 PM</b>	M. Heins, J. Carroll, M-Y. Kao, J. Delaney, and C. Campbell	
<b>TU1C-2</b>	<b>Wideband AlGaIn/GaN HEMT MMIC Low Noise Amplifier</b>	<b>153</b>
<b>1:40 PM</b>	G. Ellis, J. Moon, D. Wong, M. Micovic, A. Kurdoghlian, P. Hashimoto, and M. Hu	
<b>TU1C-3</b>	<b>High Performance and High Reliability InP HEMT Low Noise Amplifiers for Phased-Array Applications</b>	<b>157</b>
<b>2:00 PM</b>	R. Grundbacher, Y-C. Chou, R. Lai, K. Ip, S. Karn, M. Barsky, G. Hayashibara, D. Leung, D. Eng, R. Tsai, M. Nishimoto, T. Block, P-H. Liu, and A. Oki	
<b>TU1C-4</b>	<b>Cryogenic 2-4 GHz Ultra Low Noise Amplifier</b>	<b>161</b>
<b>2:20 PM</b>	A. Mellber, N. Wadefalk, I. Angelov, E. Choumas, E. Kollberg, N. Rorsman, P.J. Starski, J. Stenarson, and H. Zirath	

## Session TU2C

### Frequency Convoverion and Signal Control

Room 201BC

Chair: B. Nelson, Sirenza Microdevices

Co-chair: M. Madihian, NEC Labs America, Inc.

<b>TU2C-1</b>	<b>A DC-100 GHz Frequency Doubler in InP DHBT Technology</b>	<b>167</b>
<b>1:20 PM</b>	V. Puyal, A. Konczykowska, P. Nouet, S. Bernard, S. Blayac, F. Jorge, M. Riet, and J. Godin	
<b>TU2C-2</b>	<b>A Highly Integrated Ka- band MMIC Quadrupler</b>	<b>171</b>
<b>1:40 PM</b>	K. Kamozaiki, T. Bos, and E. Camargo	
<b>TU2C-3</b>	<b>A Frequency Doubler with High Conversion Gain and Good Fundamental Suppression</b>	<b>175</b>
<b>1:50 PM</b>	F. Gruson, G. Bergmann, and H. Schumacher	
<b>TU2C-4</b>	<b>40 and 60 GHz Frequency Doublers in 90-nm CMOS</b>	<b>179</b>
<b>2:00 PM</b>	M. Ferndahl, B.M. Motlagh, and H. Zirath	
<b>TU2C-5</b>	<b>60-GHz-band Intentional LO-leakage APDP Mixer for SSB Self-Heterodyne Transmitter Module</b>	<b>183</b>
<b>2:20 PM</b>	S. Kishimoto, K. Maruhashi, M. Ito, Y. Hamada, and K. Ohata	
<b>TU2C-6</b>	<b>A Q-band Miniaturized Uniplanar MMIC HEMT Mixer</b>	<b>187</b>
<b>2:40 PM</b>	C-H. Wang, Y-S. Lin, H. Wang, and C.H. Chen	
<b>TU2C-7</b>	<b>A Ku-band MOSFET Phase Shifter MMIC</b>	<b>191</b>
<b>2:50 PM</b>	H.D. Lee, D.W. Kang, C-H. Kim, and S. Hong	

## Session TU3C

# Novel Microwave and Millimeter-Wave Components

**Room BallC**

Chair: T. Itoh, University of California at Los Angeles

Co-chair: J. Taub, Consultant

<b>TU3C-1</b>	<b>On-Chip High-Q Cu Inductors Embedded In Wafer-Level Chip-Scale Package for Silicon RF Application</b>	<b>197</b>
<b>1:20 PM</b>	K. Itoi, M. Sato, H. Abe, H. Sugawara, H. Ito, K. Okada, K. Masu, and T. Ito	
<b>TU3C-2</b>	<b>Integrated Transmission Line Transformer</b>	<b>201</b>
<b>1:40 PM</b>	J. Horn and G. Boeck	
<b>TU3C-3</b>	<b>Si-based Inductors and Transformers for 30-100 GHz Applications</b>	<b>205</b>
<b>2:00 PM</b>	T. Dickson, M-A. LaCroix, S. Boret, D. Gloria, R. Beerkens, and S. Voinigescu	
<b>TU3C-4</b>	<b>Design of Compact Planar Antennas using LH-Transmission Lines</b>	<b>209</b>
<b>2:20 PM</b>	M. Schuessler, J. Freese, and R. Jakoby	
<b>TU3C-5</b>	<b>Compact Folded-Waveguide Resonators</b>	<b>213</b>
<b>2:40 PM</b>	J-S. Hong	

## Session TU4C

# Millimeter-Wave MMIC Components and Subsystems

**Room 202CD**

Chair: D. Choudhury, HRL Laboratories, LLC

Co-chair: E. Niehenke, Niehenke Consulting

<b>TU4C-1</b>	<b>High-Receiving-Sensitivity 70-GHz Band MMIC Transceiver: Application of Receiving-Module-Arrayed Self-Heterodyne Technique</b>	<b>219</b>
<b>1:20 PM</b>	Y. Shoji and H. Ogawa	
<b>TU4C-2</b>	<b>SiGe-Based Circuits for Sensor Applications beyond 100 GHz</b>	<b>223</b>
<b>1:40 PM</b>	M. Steinhauer, H. Irion, M. Schott, M. Thiel, H-O. Ruoss, and W. Heinrich	
<b>TU4C-3</b>	<b>Design and Analysis of a W-band Multiplier Chipset</b>	<b>227</b>
<b>2:00 PM</b>	J. Lynch, E. Entchev, B. Lyons, A. Tessmann, H. Massler, A. Leuther, and M. Schlechtweg	
<b>TU4C-4</b>	<b>W-Band InP DHBT MMIC Power Amplifiers</b>	<b>231</b>
<b>2:20 PM</b>	G. Ellis, A. Kurdoghlian, R. Bowen, M. Wetzel, and M. Delaney	
<b>TU4C-5</b>	<b>Design and Analysis of a Miniature W-Band MMIC Subharmonically Pumped Resistive Mixer</b>	<b>235</b>
<b>2:40 PM</b>	M-F. Lei, P-S. Wu, T-W. Huang, and H. Wang	

## Session TU5C

# Design and Characterization of Ferrite and Ferroelectric Devices

Room 201A

Chair: B. Elsharawy, Arizona State University

Co-chair: B. York, University of California, Santa Barbara

<b>TU5C-1</b>	<b>Numerical Studies about the Temperature Compensation of Microwave Circulators</b>	<b>241</b>
1:20 PM	T. Lingel	
<b>TU5C-2</b>	<b>Lumped Element Isolator with Lower-Symmetrical Configuration of Three Windings</b>	<b>245</b>
1:40 PM	S. Takeda, H. Mikami, and Y. Sugiyama	
<b>TU5C-3</b>	<b>Nonreciprocal Left-Handed Microstrip Lines Using Ferrite Substrate</b>	<b>249</b>
1:50 PM	M. Tsutsumi and T. Ueda	
<b>TU5C-4</b>	<b>A New Concept for Functional Electromagnetic Cell Material for Microwave and Millimeter Use</b>	<b>253</b>
2:00 PM	Y. Kotsuka and M. Armano	
<b>TU5C-5</b>	<b>Design of Ferroelectric Phase Shifters for Minimum Performance Variation over Temperature</b>	<b>257</b>
2:10 PM	D. Kim, S-S. Je, J.S. Kenney, and P. Marry	
<b>TU5C-6</b>	<b>Analog Tunable Matching Network using Integrated Thin-Film BST Capacitors</b>	<b>261</b>
2:30 PM	V. Chen, R. Forse, D. Chase, and R.A. York	
<b>TU5C-7</b>	<b>On-wafer Microwave Characterization of Ferroelectric Thin Film Phase Shifters</b>	<b>265</b>
2:40 PM	P.M. Suherman, T. Jackson, Y. Koutsonas, R.A. Chakalov, and M. Lancaster	
<b>TU5C-8</b>	<b>Microwave Measurement and Modeling of Capacitors with Tunable Dielectric Constants</b>	<b>269</b>
2:50 PM	N. Cramer, E. Philofsky, L. Kammerdiner, and T.S. Kalkur	

## Session TU6C

# Microwave Generation by Optical Techniques

Room 202AB

Chair: A. Madjar, Drexel University

Co-chair: T. Berceci, Technical University of Budapest

<b>TU6C-1</b>	<b>THz Photomixing Employing Traveling-Wave Photodetectors</b>	<b>275</b>
1:20 PM	A. Stöhr, A. Malcoci, and D. Jager	
<b>TU6C-2</b>	<b>Microwave Vector Modulation and Arbitrary Waveform Generation using Optical Techniques</b>	<b>279</b>
1:40 PM	A. Leven, J. Lin, J. Lee, U-V. Koc, K-Y. Tu, Y. Baeyens, and Y. Chen	
<b>TU6C-3</b>	<b>Optical Generation of Microwave Signals Based on an Unbalanced Fiber Loop Mirror</b>	<b>283</b>
1:50 PM	C. Schaeffer and I.G. Insua	
<b>TU6C-4</b>	<b>Progress in the Opto-Electronic Oscillator – A Ten Year Anniversary Review</b>	<b>287</b>
2:10 PM	S. Yao, L. Maleki, and D. Elyahu	
<b>TU6C-5</b>	<b>Improving the Frequency Stability and Phase Noise of Opto-Electronic Oscillators by Harmonic Feedback</b>	<b>291</b>
2:30 PM	T. Banky, T. Berceci, and B. Horvath	
<b>TU6C-6</b>	<b>Microwave Generation by Regenerative Mode-Locking of a Nd:YVO4/MgO:LiNbO3 Microchip Laser</b>	<b>295</b>
2:40 PM	A. Madjar, D. Yoo, P.R. Herczfeld, W.D. Jemison, S.M. Goldwasser, and Y. Li	

## Session TU1D

# Metamaterials: Left-Handed Materials and Transmission Lines

**3:30pm – 5:10pm**

**Room 200**

Chair: A. A. Oliner, Polytechnic University

Co-chair: J. Zehentner, Czech Technical University in Prague

<b>TU1D-1</b>	<b>A Via-Free Microstrip Left-Handed Transmission Line</b>	<b>301</b>
<b>3:30 PM</b>	A. Sanada, K. Murakami, S. Aso, H. Kubo, and I. Awai	
<b>TU1D-2</b>	<b>Leaky-Waves in a Metamaterial-Based Two-Dimensional Structure for a Conical Beam Antenna</b>	<b>305</b>
<b>3:50 PM</b>	<b>Application</b> C.A. Allen, C. Caloz, and T. Itoh	
<b>TU1D-3</b>	<b>The Nature of Radiation From Leaky Waves On Single- and Double-Negative Metamaterial</b>	<b>309</b>
<b>4:10 PM</b>	<b>Grounded Slabs</b> P. Baccarelli, P. Burghignoli, F. Frezza, A. Galli, P. Lampariello, G. Lovat, and S. Paulotto	
<b>TU1D-4</b>	<b>Electronically-Controlled Metamaterial-Based Transmission Line as a Continuous-Scanning</b>	<b>313</b>
<b>4:30 PM</b>	<b>Leaky-Wave Antenna</b> S. Lim, C. Caloz, and T. Itoh	
<b>TU1D-5</b>	<b>Nonlinear Transmission Lines in Left-Handed Media</b>	<b>317</b>
<b>4:50 PM</b>	A. Kozyrev and D. van der Weide	

## Session TU3D

# Directional Coupler Techniques

**Room BallC**

Chair: J. Owens, Boise State University

Co-chair: C. Buntschuh, Microwave Engineering Services

<b>TU3D-1</b>	<b>Design of Fractal Rat-Race Coupler</b>	<b>323</b>
<b>3:30 PM</b>	H. Ghali and T.A. Moselhy	
<b>TU3D-2</b>	<b>A Novel Compact Multi-Layer MMIC CPW Branchline Coupler Using Thin-Film Microstrip</b>	<b>327</b>
<b>3:50 PM</b>	<b>Stub Loading at 44 Ghz</b> K. Hettak, G.A. Morin, and M.G. Stubbs	
<b>TU3D-3</b>	<b>Miniaturized 90° Hybrid Circuit Using Quasi-Distributed TFMS Line</b>	<b>331</b>
<b>4:10 PM</b>	T. Tanaka, K. Nishikawa, and M. Aikawa	
<b>TU3D-4</b>	<b>Design of a 90 Hybrid Coupler with Harmonic Rejection Characteristic</b>	<b>335</b>
<b>4:30 PM</b>	S-Y. Lee, Y. Chung, T. Itoh, and D. Ahn	
<b>TU3D-5</b>	<b>Series-Configuration of Multi-Line Directional-Coupler Sections with Improved Coupling</b>	<b>339</b>
<b>4:50 PM</b>	H. Schmiedel	

## Session TU4D

# Millimeter- and Submillimeter-Wave Components and Technology

Room 202CD

Chair: R. Emrick, Motorola Labs

Co-chair: J. Wiltse, Georgia Tech

<b>TU4D-1</b>	<b>A Precision Micromachining Technique for the Fabrication of Hybrid Millimeter Wave Circuits and Sub-assemblies</b>	<b>345</b>
3:30 PM	W. Chow, A. Champion, and D. Steenson	
<b>TU4D-2</b>	<b>Micromachined Millimeter-Wave Module for Power Combining</b>	<b>349</b>
3:50 PM	Y. Lee, J. East, and L. Katehi	
<b>TU4D-3</b>	<b>Periodic Filters for Performance Enhancement of Millimeter-wave Microstrip Antenna Arrays</b>	<b>353</b>
4:10 PM	C. Eswarappa, R. Anderson, and F. Kolak	
<b>TU4D-4</b>	<b>Millimeter-Wave Corrugated Tapered-Slot Antennas</b>	<b>357</b>
4:30 PM	R. Judaschke and M. Palacios	
<b>TU4D-5</b>	<b>Terahertz-Emitting Devices Based on Boron-Doped Silicon</b>	<b>361</b>
4:40 PM	R.T. Troeger, T.N. Adam, S.K. Ray, P. Lv, S. Kim, G. Xuan, S. Ghosh, and J. Kolodzey	
<b>TU4D-6</b>	<b>Novel Possibilities for Coherent Radiation Sources</b>	<b>365</b>
4:50 PM	Y.A. Hussein and J.E. Spencer	

## Session TU5D

# Microwave Acoustic Devices

Room 201A

Chair: R. Weigel, University of Erlangen-Nuremberg

Co-chair: S. Stitzer, Northrop Grumman Electronic Systems

<b>TU5D-1</b>	<b>Bulk Acoustic Wave Filters for GPS with Extreme Stopband Attenuation</b>	<b>371</b>
3:30 PM	M. Handtmann, S. Marksteiner, J. Kaitila, and R. Aigner	
<b>TU5D-2</b>	<b>Proposal of a New Landing Area for SAW RF Filters in Wireless Applications Ensuring Precisely Predictable Filter Characteristics</b>	<b>375</b>
3:50 PM	H. Bilzer, F.M. Pitschi, J.E. Kiwitt, K.Ch. Wagner, and W. Menzel	
<b>TU5D-3</b>	<b>New Modeling of TFBAR and On-Wafer Inductor Effects on the TFBAR Ladder Filter Performance</b>	<b>379</b>
4:10 PM	J-S. Kim, Y-D. Kim, M.G. Gu, and J-G. Yook	
<b>TU5D-4</b>	<b>Electromagnetic Modeling of Thin-Film Bulk Acoustic Resonators</b>	<b>383</b>
4:20 PM	M. Farina and T. Rozzi	
<b>TU5D-5</b>	<b>Voltage Controlled SAW Filters on 2DEG AlGaIn/GaN Heterostructures</b>	<b>387</b>
4:30 PM	J. Grajal, F. Calle, J. Pedros, and T. Palacios	
<b>TU5D-6</b>	<b>Balanced Lattice-Ladder Bandpass Filter in Bulk Acoustic Wave Technology</b>	<b>391</b>
4:40 PM	H.K. Jan ten Dolle, J-W. Lobeek, A. Tuinhout, and J. Foekema	
<b>TU5D-7</b>	<b>Integration of Bulk Acoustic Wave Filters: Concepts and Trends</b>	<b>395</b>
4:50 PM	L. Elbrecht, R. Aigner, C-I. Lin, and H-J. Timme	

# Session TU6D

## Numerical Modeling for RF/Microwave Photonic Applications

Room 202AB

Chair: K. Goverdhanam, Agere Systems

Co-chair: A. Gopinath, University of Minnesota

<b>TU6D-1</b> <b>3:30 PM</b>	<b>Characteristics of InP HEMT Harmonic Optoelectronic Mixers and Their Application to 60GHz Radio-on-Fiber Systems</b> C-S. Choi, H-S. Kang, D-H. Kim, K-S. Seo, and W-Y. Choi	<b>401</b>
<b>TU6D-2</b> <b>3:50 PM</b>	<b>All-Optical Harmonic Frequency Up-Conversion for a WDM Radio Over Fiber System</b> H-J. Song, J.S. Lee, and J-I. Song	<b>405</b>
<b>TU6D-3</b> <b>4:10 PM</b>	<b>Global EM and Thermal analysis of a 40Gb/s all integrated optoelectronic transmitter module</b> B. Thon, D. Baillargeat, S. Verdeyme, and R. Lefevre	<b>409</b>
<b>TU6D-4</b> <b>4:30 PM</b>	<b>Performance Analysis of MMoF Systems Considering Laser Phase Noise under Rician Fading</b> C. Yun, T-S. Cho, S. Sung, and K. Kim	<b>413</b>
<b>TU6D-5</b> <b>4:50 PM</b>	<b>Effect of Laser and RF Oscillator Phase Noises</b> T-S. Cho, C. Yun, K. Kim, and K. Kim	<b>417</b>